ASEAN
Journal of Scientific and Technological Reports
Online ISSN:2773-8752

Research article

Leakage Current Modeling for Grounding in Single-Track Electric Mass Transit Systems

Tawat Chuchit[1], Supachai Kaewpoung[2], Wiwat Su-hren[3], Arnon Isaramongkolrak[4], and Tanawat Srirugsa[5*]

[1] Faculty of Engineering, Thaksin University, Phatthalung, 93210, Thailand
[2] Faculty of Engineering, Thaksin University, Phatthalung, 93210, Thailand
[3] Faculty of Engineering, Thaksin University, Phatthalung, 93210, Thailand
[4] Science and Technology, Nakhon Pathom Rajabhat University, Nakhon Pathom, 73000, Thailand
[5] Faculty of Engineering, Thaksin University, Phatthalung, 93210, Thailand
* Correspondence: tanawat.s@tsu.ac.th

Citation:
Chuchit, T.; Kaewpoung, S.; Su-hren, W.; Isaramongkolrak, A.; Srirugsa, T. Leakage current modeling for grounding in single-track electric mass transit systems. *ASEAN J. Sci. Tech. Report.* **2025**, *28*(3), e257546. https://doi.org/10.55164/ajstr.v28i3.257546.

Article history:
Received: January 17, 2025
Revised: April 3, 2025
Accepted: April 19, 2025
Available online: April 26, 2025

Abstract: This study utilizes MATLAB/Simulink to analyze leakage current in the DC electric train power supply system. The objective is to develop simulation models using MATLAB/Simulink to evaluate and compare the simulation results with mathematical and discrete models. The study focuses on three simulation models with a drainage diode: FNRCS, SCCNS, and SCCNS. It examines leakage current behavior and assesses rail voltage characteristics over a distance of 0 to 5.00 km. The simulation results for the FNRCS model indicated a voltage drop from 169.90 V at the initial point to -297.38 V at 5.00 km, along with an increase in leakage current to 14.82 A. These findings align with both the discrete and mathematical models. Compared to the mathematical model, the average increase in leakage current was 40.07%. The simulation results for the SCCNS exhibited behavior similar to that of the FNRCS in terms of both rail voltage and leakage current. The average rail voltage of the SCCNS with a drainage diode was 284.62 V, demonstrating a steady decline. However, the leakage current increased significantly with distance. Compared to the SCCNS, SCCNS with a drainage diode exhibited higher rail voltage in the 0-3.00 km range and lower rail voltage in the 3.00-5.00 km range. The development of MATLAB/Simulink models for the railway power supply system has proven to be a practical approach for analyzing rail voltage and leakage current, offering valuable insights compared to discrete and mathematical models.

Keywords: Leakage current; Rail voltage; MATLAB/Simulink; DC electric rail transit systems

1. Introduction

Power supply systems for electric railroads are now being developed further to improve system efficiency. Consequently, more and more specialist researchers are adopting computer simulation tools to create models. This strategy is becoming more popular because it is difficult to test or alter systems because of the high cost and lengthy installation time, particularly when making changes to the system. For long-term implementation, however, research on minimizing electrical leakage in railway systems has emerged as a crucial component of system analysis [1]. Various study approaches and methodologies are used to understand the effects of electrical leakage and suggest ways to reduce the dangers involved. To evaluate the behavior of electrical leakage in various systems, such as predicting the impacts of soil resistance through simulations, these studies frequently employ numerical approaches and mathematical models [2-3]. Furthermore, designs aimed at lowering the hazards

of leaking to the structural integrity of the rails are being developed as part of recommendations for managing electrical leakage in both above-ground and underground railway systems [4-5].

However, Studies of these systems also emphasize how crucial it is to use the right materials and technologies to lower energy loss and improve rail transport systems' safety [6-7]. Furthermore, enhancing railway power supply systems requires assessing the use of materials to reduce electrical leakage [8] and creating methods for identifying electrical leakage in railway transport systems [9]. These efforts aid in developing detection systems and maintenance procedures to monitor electrical leakage precisely [10]. Additionally, electrical leakage analysis in railway power supply systems is essential for advancing and enhancing railway transport systems, especially regarding safety and reducing energy losses in the electrical network [11-12]. The behavior of electrical leakage in three different simulated scenarios has been studied and compared using MATLAB/Simulink simulation tools. A comparison between mathematical and commercially available simulation models has also been conducted [13]. The conductivity between the soil and rails is a crucial factor in determining the features of the leakage current and rail voltage, as evidenced by the findings of earlier research that showed notable variations in the incidence of electrical leakage in each situation [14-15].

Understanding how different environmental conditions, such as humidity, temperature, and rail design, affect electrical leakage requires parameter modeling techniques [16-17]. This emphasizes the necessity of creating new models to help with more accurate calculations and electrical leak detection. Furthermore, studies have concentrated on reducing electrical leakage using novel materials and technologies, which may enhance intercity railway power systems [18-19]. Another important area of study is the effect of electrical leaks on rail structures and how to identify leaks caused by poor design [20-21]. These studies offer strategies for creating maintenance and detection systems that lower the hazards of electrical leaks [22]. These studies, which use engineering analysis and simulation methodologies, are crucial for planning and creating future electrical systems that are safer, more efficient, and more effective, in addition to helping to understand how electrical leakage behaves in electric rail systems. Research in this area is crucial to further the development of high-performance electric rail systems. It focuses on energy-efficient electrical system design, electrical leakage behavior simulation, and guaranteeing safety in future railway transport systems [23-34].

The Direct Current (DC) Railway System is still widely used in many cities worldwide. It was created to ease traffic congestion and promote public transit. The third rail in this system provides power to the trains, while the running rail acts as the driving current's return conductor. Some electrical current leaks or stray currents return to the power station through the ground due to insufficient insulation between the running rail and the ground [25]. Since it is usually challenging to monitor stray currents directly, voltage variations between the ground and the running rail are usually measured instead. The rail potential is the name given to this voltage differential. Furthermore, stray currents are dangerous since, according to the EN-50122-1 standard for DC railway systems, the voltage that can be touched should not be higher than 120 V for longer than 300 seconds. Following EN-50122-2, the rail's voltage shall not surpass 5 V in a 24-hour period [26-28]. Evaluating and regulating the rail voltage is crucial to avoid or lessen such harm. As a result, it is essential to build models for assessing rail voltage and carry out basic research for these evaluations [29-32].

This study aims to create a MATLAB/Simulink model of the electric railway track power supply system to examine leakage current and rail potential voltage. (Figure 1), depicts a DC traction system, which serves as the model's starting point. The EN-50122-2 standard is followed in the design of the railway system's bonding and earthing. Furthermore, the model is constructed following the guidelines for electric train power supply systems, integrating the models of the FNRCS, the SCCNS, and the SCCNS with a drainage diode. The variations in leakage current and rail potential voltage within the system under study are compared using these models.

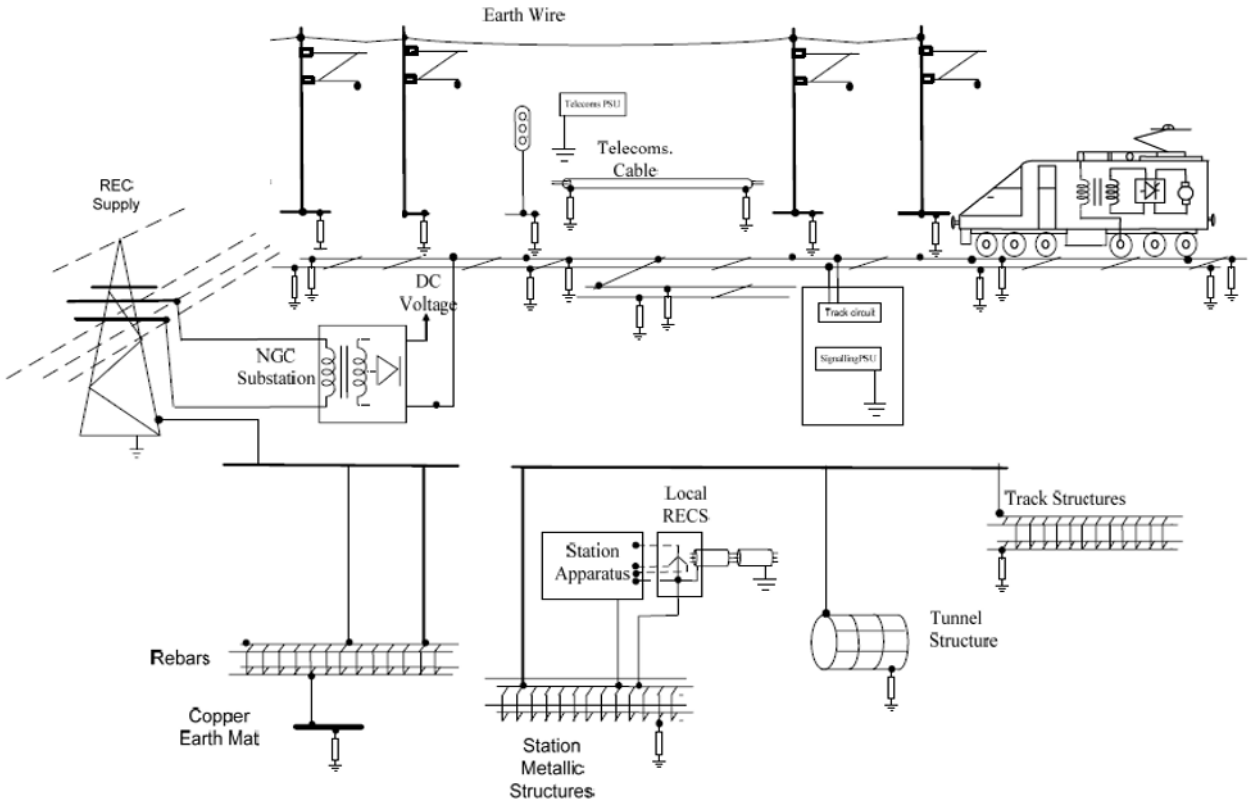

Figure 1. Structural earthing and bonding in the railway system with EN-50122-2 [33].

This grounding setup for DC electric train power supply systems is called the Rail Insulation System (RIS) and its construction (Figure 1). Electric current returns to the power substation via the train wheels and running rails in this arrangement. Due to the absence of electrical insulation between the running rails and the sleepers or other supporting structures, stray currents could seep into different areas of the infrastructure in traditional railway systems. As a result, there were intricate and challenging alternative return routes. To mitigate this problem, contemporary railway systems have integrated electrical insulation between the running rails and supporting elements. This has been shown to minimize corrosion of metallic structures and effectively reduce stray current leakage. The conductance per unit length between the ground and the running rails (track-to-earth) should not be greater than 500 mS/km for open formation systems and 2500 mS/km for closed formation systems, according to the EN-50122-2 standard. To ensure that every component is correctly grounded following EN-50122-2, the system also calls for improved earthing and bonding of metallic structures and reinforced concrete components. Installing low-resistance rail joint bonds across the rail network is necessary to reduce voltage drops along the rails further. The total rail resistance cannot rise by more than 5% due to the extra resistance these bonds add. Both running rails in double-track railway systems need to be connected to ensure efficient current return pathways. Improved safety and operational efficiency are guaranteed by the widespread adoption of this system configuration on Network Rail's DC railway networks in the UK (United Kingdom).

2. Theories and Mathematical models

A thorough grasp of basic ideas and concepts is necessary to create a model for evaluating different electrical parameters in the electric train power supply system. These are necessary for simplifying the process and computing the parameters using simple equations from the system's single-line diagram model. Computer programming tools are used to produce precise calculations while reducing computation complexity and time. The two primary sections of this section address the pertinent theories and mathematical models of the electric train power supply system. According to the established standards, the first section discusses the DC electric traction system's structure and methods for determining leakage current and voltage.

The main topics of the second section are the tractive force of the train and the properties of the electrical power needed for train motion. Both sections are essential for creating a model with MATLAB/Simulink, a computer program that effectively computes the necessary values.

2.1 DC Traction Earthing System

The DC Traction Earthing System, a grounding system structure of the DC traction system, is essential for controlling and managing the return current that flows from the traction motors back to the power source. This is crucial for improving railway operations' efficiency and guaranteeing operational safety. The three main types of systems are the floating negative return current system (FNRCS), the sty current collecting net system (SCCNS), and the SCCNS with a drainage diode. Each system functions according to certain principles to safely control return currents and preserve DC railway systems' functionality.

2.1.1. FNRCS

The negative busbar is not grounded from the rectifier substation's output in the FNRCS design. Because the substation isn't directly connected to the ground, the voltage at the negative busbar floats and doesn't always stay at zero. High touch voltage is more likely in this setup, which could endanger operational staff or living things who might unintentionally come into contact with the system. Additional rail potential control devices must be installed to manage the rail voltage and reduce this risk. This configuration of the system (Figure 2). Hong Kong's LRT and Singapore's MRT are two notable train systems that use this basic technique. This article simulates the FNRCS system using a remote ground for grounding, which has an approximate value of zero ohms, as per the RIS.

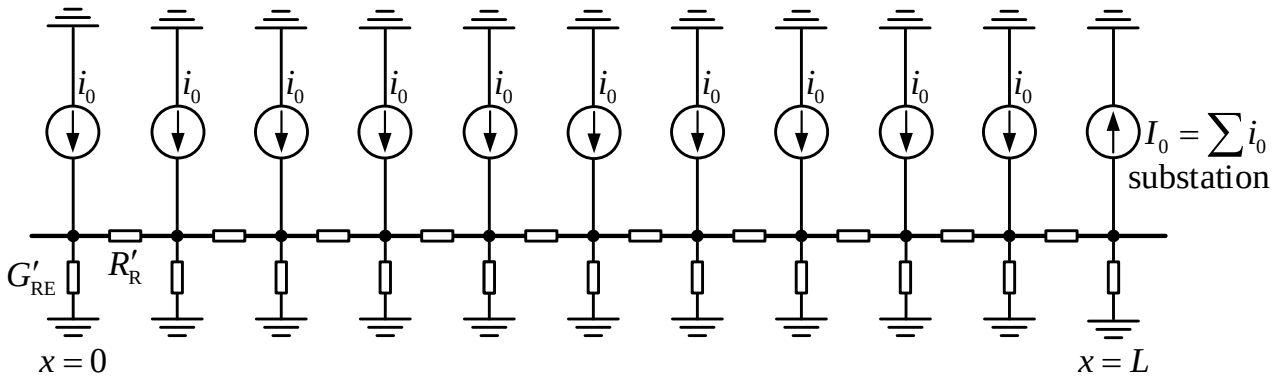

Figure 2. Circuit diagram for FNRCS.

Concerning the non-continuous (discrete) distribution of current sources in the FNRCS, (Figure 2) depicts the structure of discretely distributed current sources. The purpose of this setup is to effectively regulate and control the flow of return current in a DC traction system. Reducing stray current leakage into the ground and preventing corrosion of metallic infrastructure elements, like underground pipelines and railroad tracks, are the goals of the discrete distribution of current sources. The system structure has been converted into a mathematical analysis scheme to efficiently examine and compute the electrical behavior within the FNRCS (Figure 3). This transformation makes it easier to depict how the system operates mathematically by representing the discrete current sources as mathematical current sources. This method makes analyzing the distribution of voltage and current throughout the system easier and more systematic. Additionally (Figure 4), the FNRCS structure's mathematical modeling makes it possible to create an equivalent circuit for assessing the possible drop along a section of railroad track. This analogous circuit faithfully simulates the behavior of electrical currents and voltages across different system components. It usually consists of current sources that replicate return currents and possible stray currents, as well as resistors that represent the resistance of the rails and wires.

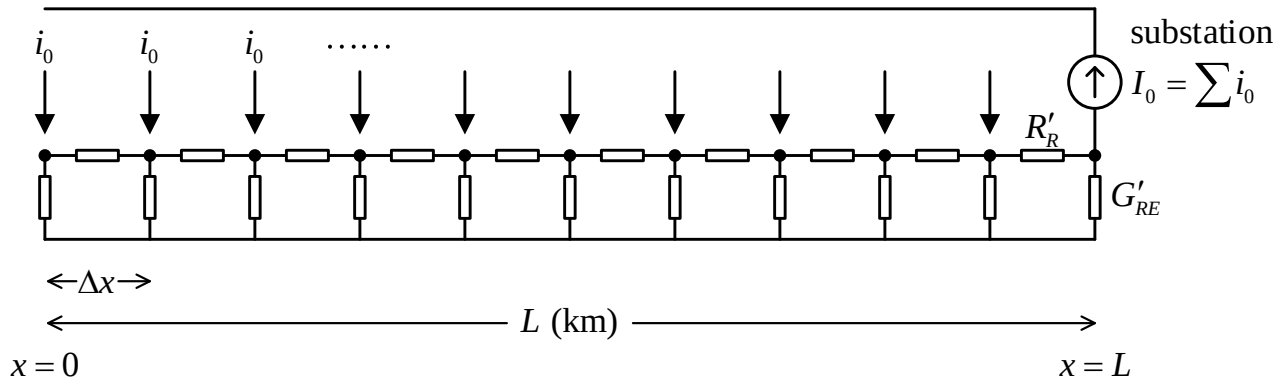

Figure 3. Circuit diagram scheme for the mathematical model.

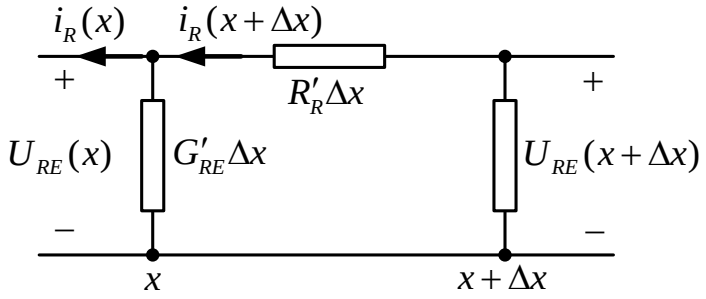

Figure 4. Potential drop along a track element

Using Kirchhoff's voltage law, which is represented in equation (1), the analysis may be completed from (Figure 4). Equation (2) illustrates how to rewrite the problem by setting (), and equation (3) is also obtained by applying Kirchhoff's current law at node (x). Equation (4) can be obtained by further simplifying the equation when ($\Delta x \to 0$), equation (5) is the final result of taking the derivative of equation (4) concerning (x).

$$-U_{RE}(x+\Delta x)+i_R(x+\Delta x)R'_R\Delta x+U_{RE}(x)=0 \tag{1}$$

$$\frac{dU_{RE}(x)}{dx}=i_R(x)R'_R \tag{2}$$

$$i_R(x+\Delta x)=U_{RE}(x)G'_{RE}\Delta x+i_R(x) \tag{3}$$

$$\frac{di_R(x)}{dx}=U_{RE}(x)G'_{RE} \tag{4}$$

$$\frac{d^2i_R(x)}{dx^2}=\frac{dU_{RE}(x)}{dx}G'_{RE} \tag{5}$$

The result of reformatting equation (5) after substituting equation (2) is equation (6). Equation (7), which is obtained by further rearranging the equation with ($\alpha = \sqrt{R'_R G'_{RE}}$), is obtained. As a result, the form given in equation (8) is used to get the answer for the second-order derivative. If (L) is the length of the distance interval under discussion, and (x) is the beginning point at the power supply station (Figure 3), then (A) and (B) may be

found using the conditions at (x = 0) and (x = L), which are (At x = 0: $i_R(0)=0$) and (At x = L: $i_R(L)=I_0=i_0L$). Subsequently, the equations are rewritten as (9) and (10).

$$\frac{d^2i_R(x)}{dx^2}=i_R(x)R'_RG'_{RE}=\alpha^2i_R(x) \tag{6}$$

$$\frac{d^2I_R(x)}{dx^2}-\alpha^2I_R(x)=0 \tag{7}$$

$$i_R(x)=Ae^{\alpha x}+Be^{-\alpha x} \tag{8}$$

$$0=A+B\rightarrow A=-B \tag{9}$$

$$i_0L=Ae^{\alpha L}+Be^{-\alpha L} \tag{10}$$

The equations in (4) and (5) are changed to solve for (A) and (B). Equations (12) and (13) are obtained by reformatting equation (11) and substituting it into equation (8). Following that, the leakage current at position (x) that flows from the rail through the soil at a distance (x) is represented by the current (i_l (x)), which is then computed. Equation (14) is the new formulation of the equation.

$$A=\frac{i_0L}{e^{\alpha L}-e^{-\alpha L}}\ \text{ and }\ B=-\frac{i_0L}{e^{\alpha L}-e^{-\alpha L}} \tag{11}$$

$$i_R(x)=\frac{i_0L}{e^{\alpha L}-e^{-\alpha L}}e^{\alpha x}-\frac{i_0L}{e^{\alpha L}-e^{-\alpha L}}e^{-\alpha x}=\frac{i_0L}{e^{\alpha L}-e^{-\alpha L}}\left(e^{\alpha x}-e^{-\alpha x}\right) \tag{12}$$

$$i_R(x)=\frac{i_0L}{\sinh(\alpha L)}\sinh(\alpha x) \tag{13}$$

$$i_l=i_0x-i_x=i_0x-\frac{i_0L\sinh\alpha x}{\sinh\alpha L} \tag{14}$$

The leakage current ($i_{l\max}$) is then computed by setting the voltage at point (N) to zero, as stated in equation (15). Equation (16) illustrates the reformed equation. Furthermore, equation (17) provides the rail's voltage ($U_{RE}(x)$) at a distance (x) from the power supply station.

$$N=\frac{1}{\alpha}\cosh^{-1}\frac{\sinh\alpha L}{\alpha L} \tag{15}$$

$$i_{l\max}=i_0\frac{1}{\alpha}\cosh^{-1}\frac{\sinh\alpha L}{\alpha L}-\frac{i_0L}{\sinh\alpha L}\sqrt{\frac{\sinh^2\alpha L}{\alpha^2L^2}-1} \tag{16}$$

$$U_{RE}(x) = \frac{1}{G'_{RE}} \frac{di_l}{dx} = \frac{i_0}{G'_{RE}} \left(1 - \frac{\alpha L}{\sinh \alpha L} \cosh \alpha x \right) \tag{17}$$

Moreover, the computational process is made simpler by using mathematical model analysis. Equation (17) can be used to compute the voltage mathematically, and equation (18) can be used to define the node analysis approach, which determines the current at any position (x).

$$i_R(k+1) = \frac{U_{RE}(k+1) - U_{RE}(k-1)}{R'_R \Delta x} \tag{18}$$

2.1.2. SCCNS

For electric train systems that run on elevated structures or in tunnels, the SCCNS was created especially. This technique installs an SCCNS inside the tunnel or raised structure to stop metallic components from corroding. Furthermore, the net is positioned between the structure and the running rails, and it has incorporated diodes to help return stray currents to the power substation. According to additional research on this system, touch voltage can be increased about two times when an SCCNS is used, as opposed to when the net is not used. The Bangkok Transit System (BTS), created and built by SIEMENS, is a noteworthy case study. By contrasting two configurations, one with metallic bonding in the reinforced concrete structure and another with installing the SCCNS with a drainage diode, SIEMENS assessed the possible effects of stray currents in the elevated structure during the design phase (Figure 5). Stray current levels increased by up to ten times after the SCCNS was implemented, according to the results. Therefore, instead of using drainage diodes or an SCCNS, the BTS constructor chose to ground the metallic elements of the reinforced concrete structure. Based on these results, SIEMENS also advised against using drainage diodes to mitigate stray currents because of their inefficiency in lessening their effects [34].

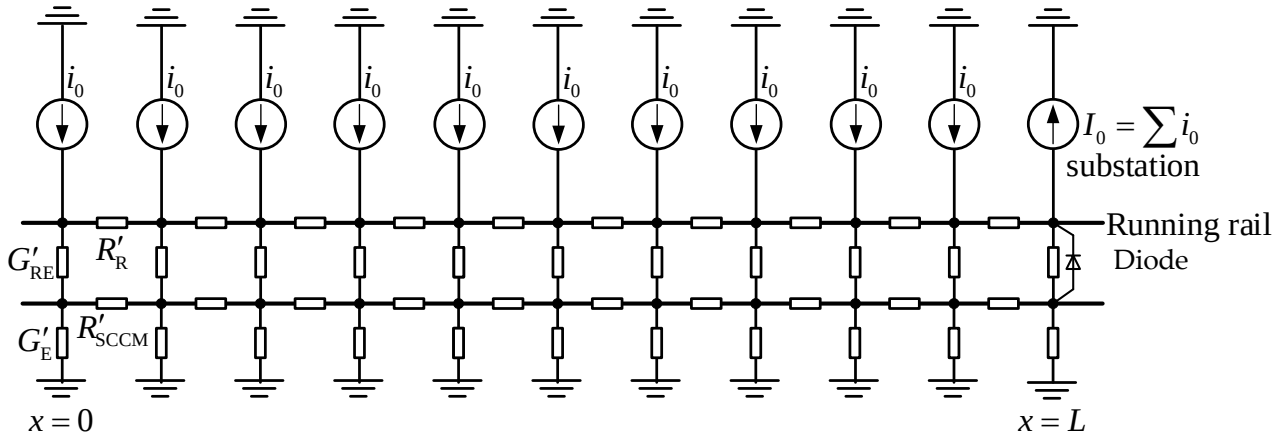

Figure 5. Circuit diagram for SCCNS with a drainage diode.

Installed the SCCNS system in diode-connected and non-diode-connected variants (Figure 5). Equation (19) illustrates how this arrangement uses node analysis to determine the link between (I) and (V). Based on standard standards, this method can be used for basic comparison analysis. (Figure 6), the complex and intricate equations are solved using the matrix form (G). Furthermore, the matrix formulations for the diode-connected and non-diode-connected scenarios are given by equations (20) and (21), respectively, when $I_n^{(R)}$, $I_{n+1}^{(s)}$ is the current entering and exiting node n via the running rail and ground structure, $G_{n,n}$ is represents

conductance at position $n \times n$, $V_n^{(R)}$, $V_{n+1}^{(S)}$ is the voltage at node n via the running rail and ground structure and V_d is the voltage across the diode.

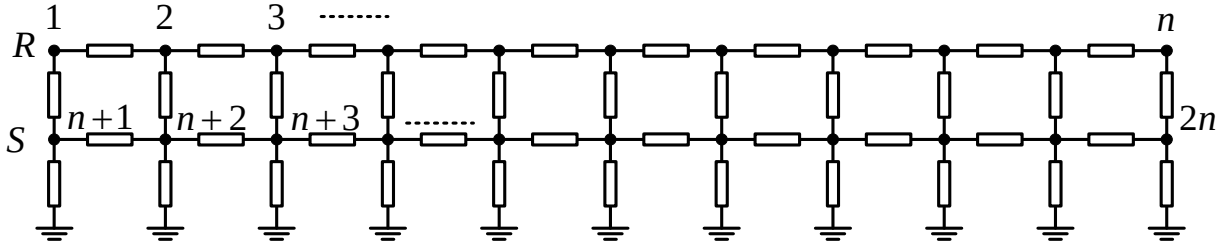

Figure 6. Circuit diagram scheme for mathematical SCCNS model.

$$[I] = [G][V] \tag{19}$$

$$\begin{bmatrix} I_1^{(R)} \\ I_2^{(R)} \\ \vdots \\ I_N^{(R)} \\ I_{n+1}^{(S)} \\ I_{n+2}^{(S)} \\ \vdots \\ I_{2n}^{(S)} \end{bmatrix} = \begin{bmatrix} G_{1,1} & G_{1,2} & \cdots & G_{1,n} & G_{1,n+1} & G_{1,n+2} & \cdots & G_{1,2n} \\ G_{2,1} & G_{2,2} & \cdots & G_{2,n} & G_{2,n+1} & G_{2,n+2} & \cdots & G_{2,2n} \\ \vdots & \vdots & \ddots & \vdots & \vdots & \vdots & \ddots & \vdots \\ G_{n,1} & G_{n,2} & \cdots & G_{n,n} & G_{n,n+1} & G_{n,n+2} & \cdots & G_{n,2n} \\ G_{n+1,1} & G_{n+1,2} & \cdots & G_{n+1,n} & G_{n+1,n+1} & G_{n+1,n+2} & \cdots & G_{n+1,2n} \\ G_{n+2,1} & G_{n+2,2} & \cdots & G_{N+2,n} & G_{n+2,n+1} & G_{n+2,n+2} & \cdots & G_{n+2,2n} \\ \vdots & \vdots & \ddots & \vdots & \vdots & \vdots & \ddots & \vdots \\ G_{2n,1} & G_{2n,2} & \cdots & G_{2n,n} & G_{2n,n+1} & G_{2n,n+2} & \cdots & G_{2n,2n} \end{bmatrix} \begin{bmatrix} V_1^{(R)} \\ V_2^{(R)} \\ \vdots \\ V_n^{(R)} \\ V_{n+1}^{(S)} \\ V_{n+2}^{(S)} \\ \vdots \\ V_{2n}^{(S)} \end{bmatrix} \tag{20}$$

$$\begin{bmatrix} I_1^{(R)} \\ I_2^{(R)} \\ \vdots \\ I_n^{(R)} \\ I_{n+1}^{(S)} \\ I_{n+2}^{(S)} \\ \vdots \\ I_{2n}^{(S)} \\ V_d \end{bmatrix} = \begin{bmatrix} G_{1,1} & G_{1,2} & \cdots & G_{1,n} & G_{1,n+1} & G_{1,n+2} & \cdots & G_{1,2n} & 0 \\ G_{2,1} & G_{2,2} & \cdots & G_{2,n} & G_{2,n+1} & G_{2,n+2} & \cdots & G_{2,2n} & 0 \\ \vdots & \vdots & \ddots & \vdots & \vdots & \vdots & \ddots & \vdots & \vdots \\ G_{n,1} & G_{n,2} & \cdots & G_{n,n} & G_{n,n+1} & G_{n,n+2} & \cdots & G_{n,2n} & 1 \\ G_{n+1,1} & G_{n+1,2} & \cdots & G_{n+1,n} & G_{n+1,n+1} & G_{n+1,n+2} & \cdots & G_{n+1,2n} & 0 \\ G_{n+2,1} & G_{n+2,2} & \cdots & G_{n+2,n} & G_{n+2,n+1} & G_{n+2,n+2} & \cdots & G_{n+2,2n} & 0 \\ \vdots & \vdots & \ddots & \vdots & \vdots & \vdots & \ddots & \vdots & \vdots \\ G_{2n,1} & G_{2n,2} & \cdots & G_{2n,n} & G_{2n,n+1} & G_{2n,n+2} & \cdots & G_{2n,2n} & -1 \\ 0 & 0 & \cdots & 1 & 0 & 0 & \cdots & -1 & 0 \end{bmatrix} \begin{bmatrix} V_1^{(R)} \\ V_2^{(R)} \\ \vdots \\ V_n^{(R)} \\ V_{n+1}^{(S)} \\ V_{n+2}^{(S)} \\ \vdots \\ V_{2n}^{(S)} \\ IV_d \end{bmatrix} \tag{21}$$

2.2 Driving of trains in railway systems.

Electric train motion is taken into account by the drive system. Depending on the manufacturer's technology, the electric train's driving motor could be an induction, synchronous, or DC motor. The general motion of the electric train set is the main emphasis of the modeling used to drive it. The traction force, the gradient force, and the electric train's resistance are the main forces driving the motion. (Figure 7) shows how the motion of the electric train was calculated and the forces at play. Equation (22) illustrates Newton's second rule of motion, which serves as the foundation for the fundamental equation used to examine the velocity of the electric train.

The following definitions of the various parameters are derived (Figure 7) and equation (22). (M_{eff}) represents the effective vehicle mass (kg), (TE) represents the tractive effort (N),(T_R) represents the train resistance (N),(F_{grad}) represents the gradient force (N), and (α) represents the train acceleration (m/s²), where an is positive for uphill motion and negative for downhill motion [35-36].

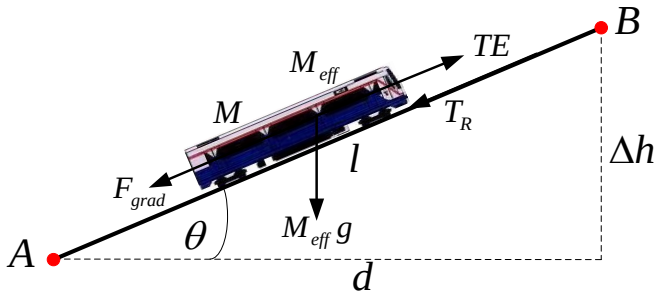

Figure 7. Computerized model for assessing train traction force [35-36].

$$F = TE - F_{grad} - T_R = M_{eff}\alpha \tag{22}$$

2.2.1. Tractive effort

The electric locomotive has traction motors to move the train. As a result, the electric locomotive's tractive force must be described for the simulation. This entails using the motor's torque-speed curve directly, where the torque from the motor is converted into tractive force and sent to the wheels via a gear reduction mechanism. The motion of the electric train can be calculated using the resulting tractive force, which the gear ratio has modified. Depending on the train's linear velocity in meters per second (m/s) or kilometers per hour (km/h), the electric train's tractive force graph, which is measured (N), changes. The figure shows the graph as dashed lines at various motor speeds. Plotting of the resulting tractive force with the horizontal axis converted to linear speed occurs after the gear ratio has been modified to account for the wheel radius and gear transmission efficiency. This results in the electric train's tractive force curve (Figure 8).

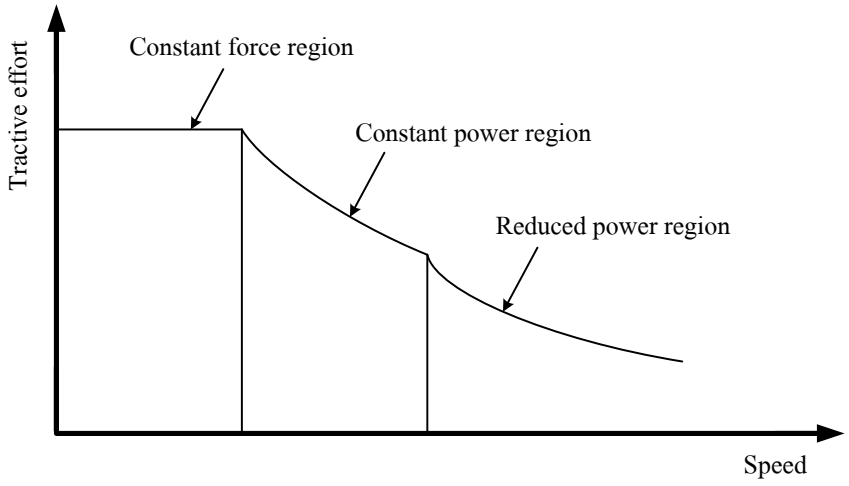

Figure 8. The tractive force of train propulsion and rotational speed of the traction motor.

2.2.2. Gradient force

Separate consideration is also given to the gravitational force acting at an inclined angle to the ground. A portion of the train's weight acts on the electric train due to its mass as it moves on a track angled on the ground. According to equation (23), this force can either support or oppose the train's motion. Additionally,

the effective weight of the electric train can be computed using equation (24), in which the passenger mass factor is indicated by (λ_w) and the tare weight is represented by (M_t).

$$F_{grad} = \pm M_{eff}\, g \sin\theta \tag{23}$$

$$M_{eff} = M_t(1+\lambda_w) \tag{24}$$

2.2.3. Train resistance

Generally speaking, the motion of a train encounters resistive forces from air resistance and wheel-rail friction, which are combined to form the resistive force. Equation (25) can be used to determine the train's total resistance. The train's speed (km/h) is represented by (v), and the constant Davis coefficients are (A: kN), (B: kN·h/km), and (C: kN·h²/km²).

$$T_R = A + Bv + Cv^2 \tag{25}$$

2.2.4. Operating Modes of Electric Trains

The operation uses the train's speed-time curve's properties to manage the movement of a train to carry people between two stations. (Figure 9), the train can be operated in four fundamental modes: coasting, braking, cruising or constant-speed, and accelerating. The train's operation may alternate between various modes depending on the intended goals. For example, the train may switch between coasting and accelerating modes to maximize energy efficiency and reduce energy consumption.

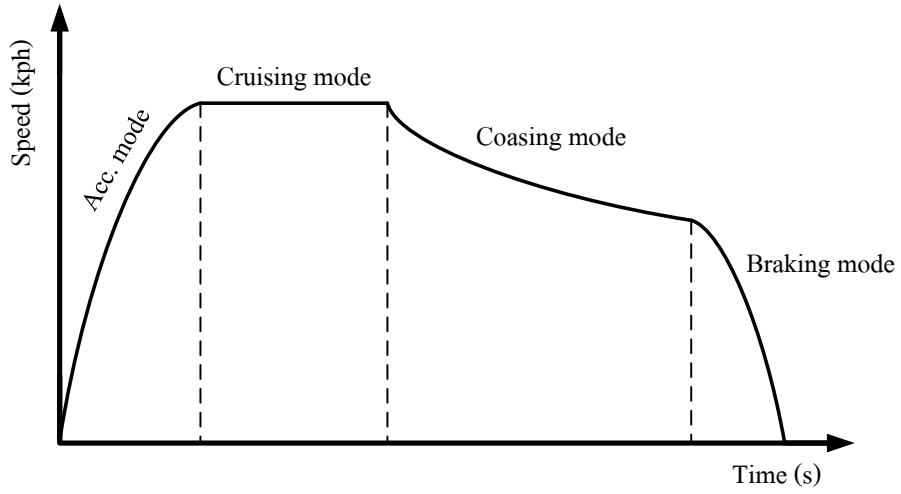

Figure 9. Characteristics of operating modes of electric trains.

According to (Figure 9), the train's operational modes determine the tractive force in each mode, which is determined by the control method. While in the accelerating mode, the train starts to accelerate from the station at a predetermined rate until it achieves the service speed. The train's acceleration is positive during this period ($\alpha_{acc} > 0$), and equation (22) can be used to determine the tractive force. After the train achieves the service speed, it enters the constant-speed mode, which keeps the speed constant until it reaches the coasting mode starting point (L_{coast}), where ($\alpha_{acc} = 0$). In the coasting mode, acceleration becomes negative, and the tractive effort drops to zero ($TE = 0$). On the other hand, when descending a steep hill, the acceleration may be positive. When the train reaches the specified braking distance or the necessary speed, it applies a negative acceleration ($\alpha_{dec} < 0$) and enters the braking mode. The tractive force, train velocity, and the effectiveness of converting mechanical energy to electrical energy (η)affect how much electric power (P : kW)

is needed to move the train. This can be calculated using equation (26). Additionally, equation (27) illustrates how the relationship can be written in terms of the substation current (I_0: A) and voltage (V_0 : V).

$$P = \frac{TE \times v}{\eta} \tag{26}$$

$$I_0 = \frac{P}{V_0} \tag{27}$$

3. Methodology and Simulation results

This study analyzes leakage current in the electric rail supply system using simulation techniques with MATLAB/Simulink. The intricacy and large-scale factors required to describe the electric rail supply system led to the selection of MATLAB/Simulink. The FNRCS, the SCCNS, and the SCCNS with a drainage diode are the three scenarios that make up the simulation. Using the single-line diagram format, the modeling procedure in all three cases closely adheres to the design and installation guidelines specified in EN-50122-2. These models are then created in MATLAB/Simulink to examine the simulation outcomes. Nevertheless, the three models, FNRCS, SCCNS, and SCCNS with a drainage diode, are commonly employed in current applications. Every model possesses distinct features that render it appropriate for different case studies. These models were chosen as the primary case studies for this research due to their effectiveness in analyzing real-world systems. This holds especially when the models are applied to analyze system behavior in actual environmental contexts. By choosing these models, one can gain a clearer insight into how the system functions and provide analysis results that are precise and applicable to actual circumstances. The following sections provide a methodical presentation of the specific simulation steps.

3.1 Simulation FNRCS model

The simulation settings are listed in the appendix (Table 8) for the FNRCS model (Figure 3), which analyzes the electric rail supply system's leakage current and voltage characteristics. The appendix (Table 7) lists the MATLAB/Simulink tools used to design and simulate these parameters. The FNRCS model was created for MATLAB/Simulink analysis, as shown in the appendix (Figure 19). To compare the outcomes of the discrete and mathematical models, this system was simulated using MATLAB/Simulink. The simulation results for voltage characteristics from the discrete model, mathematical model, and MATLAB/Simulink are presented in (Table 1) and (Table 2), respectively, when the conductance between the rail and earth was set to 0.01 S/km (for good insulation conditions) and 0.10 S/km (for insulation degradation or rainy conditions). Furthermore, (Table 3) and (Table 4), respectively, exhibit the simulation findings for leakage current.

Table 1. The rail voltage results are 0.01 S/km based on the conductance to earth FNRCS model.

No.	Distance (km)	Rail voltage (V)		
		Mathematical model	Discrete model	MATLAB/Simulink
1	0	141.5965	169.8978	169.8978
2	0.50	137.3494	161.4050	161.4050
3	1.00	124.6083	144.4191	144.4191
4	1.50	103.3723	118.9393	118.9393
5	2.00	73.6407	84.9646	84.9646
6	2.50	35.4123	42.4935	42.4935
7	3.00	-11.3147	-8.4758	-8.4758
8	3.50	-66.5422	-67.9455	-67.9455
9	4.00	-130.2726	-135.9180	-135.9180
10	4.50	-202.5085	-212.3964	-212.3964
11	5.00	-283.2531	-297.3837	-297.3837

Table 2. The rail voltage results are 0.10 S/km based on the conductance-to-earth FNRCS model.

No.	Distance (km)	Rail voltage (V)		
		Mathematical model	Discrete model	MATLAB/Simulink
1	0	140.9674	168.9832	168.9832
2	0.50	136.7472	160.5550	160.5550
3	1.00	124.0848	143.6951	143.6951
4	1.50	102.9749	118.3962	118.3962
5	2.00	73.4084	84.6476	84.6476
6	2.50	35.3728	42.4351	42.4351
7	3.00	-11.1480	-8.2595	-8.2595
8	3.50	-66.1739	-67.4575	-67.4575
9	4.00	-129.7282	-135.1843	-135.1843
10	4.50	-201.8380	-211.4684	-211.4684
11	5.00	-282.5338	-296.3425	-296.3425

Table 3. The leakage current results are 0.01 S/km based on the conductance to earth FNRCS model.

No.	Distance (km)	Leakage current (A)		
		Mathematical model	Discrete model	MATLAB/Simulink
1	0	0.0000	0.0000	0.0000
2	0.50	0.7009	0.8495	0.8495
3	1.00	1.3593	1.6565	1.6565
4	1.50	1.9328	2.3786	2.3786
5	2.00	2.3789	2.9733	2.9733
6	2.50	2.6551	3.3981	3.3981
7	3.00	2.7189	3.6106	3.6106
8	3.50	2.5278	3.5682	3.5682
9	4.00	2.0393	3.2285	3.2285
10	4.50	1.2109	2.5489	2.5489
11	5.00	0.0000	1.4869	1.4869

Table 4. The leakage current results are 0.10 S/km based on the conductance to earth FNRCS model.

No.	Distance (km)	Leakage current (A)		
		Mathematical model	Discrete model	MATLAB/Simulink
1	0	0.0000	0.0000	0.0000
2	0.50	6.9780	8.4492	8.4492
3	1.00	13.5340	16.4769	16.4769
4	1.50	19.2457	23.6617	23.6617
5	2.00	23.6906	29.5815	29.5815
6	2.50	26.4454	33.8139	33.8139
7	3.00	27.0864	35.9356	35.9356
8	3.50	25.1889	35.5226	35.5226
9	4.00	20.3269	32.1498	32.1498
10	4.50	12.0734	25.3905	25.3905
11	5.00	0.0000	14.8171	14.8171

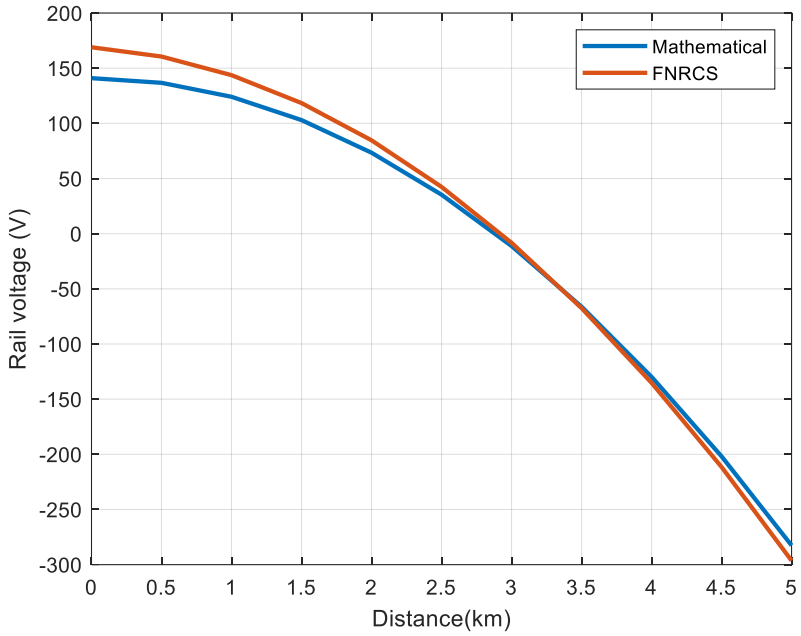

Figure 10. Results in conductance between the rail and earth by varying the rail voltage for the FNRCS model.

Voltage characteristics of the rail were evaluated and compared from (Table 1), which shows the simulation results with the conductance between the rail and earth set at 0.01 S/km for the FNRCS model, and (Table 2), where the conductance is set at 0.10 S/km. The discrete model and the simulation results from MATLAB/Simulink agreed. Consequently, the results of the discrete model were compared to those of the mathematical model. (Figure 10) shows the characteristics of rail voltage. The findings of the comparative simulation indicated an average percentage difference of 8.64% for 0.01 S/km and 8.47% for 0.10 S/km.

Furthermore, by contrasting the discrete and mathematical models, the simulation results for leakage current were examined, as indicated in (Table 3), with the conductance between the rail and earth fixed at 0.01 S/km. The discrete model's results and MATLAB Simulink's simulation results agreed. As seen in (Figure 11), this comparison showed that the leakage current rose by an average of 40.07%.

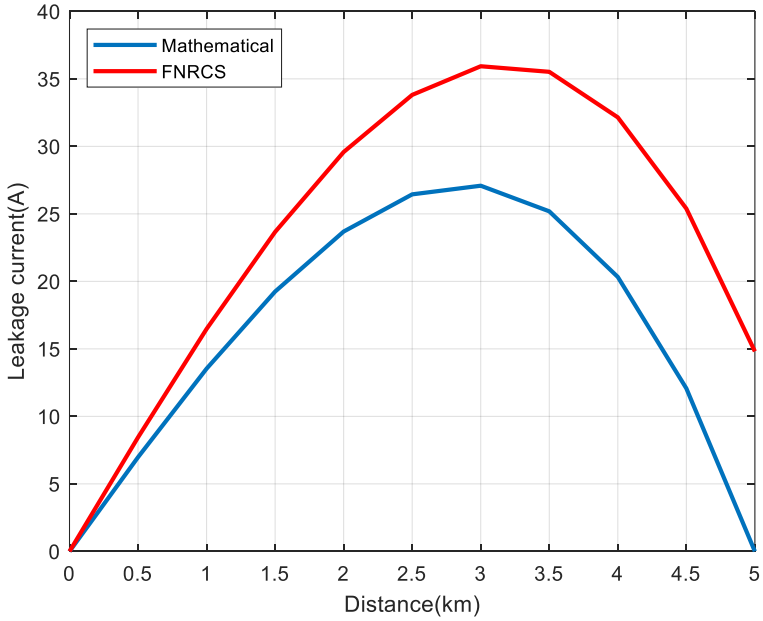

Figure 11. Results leakage current between discrete and mathematical models for the FNRCS model.

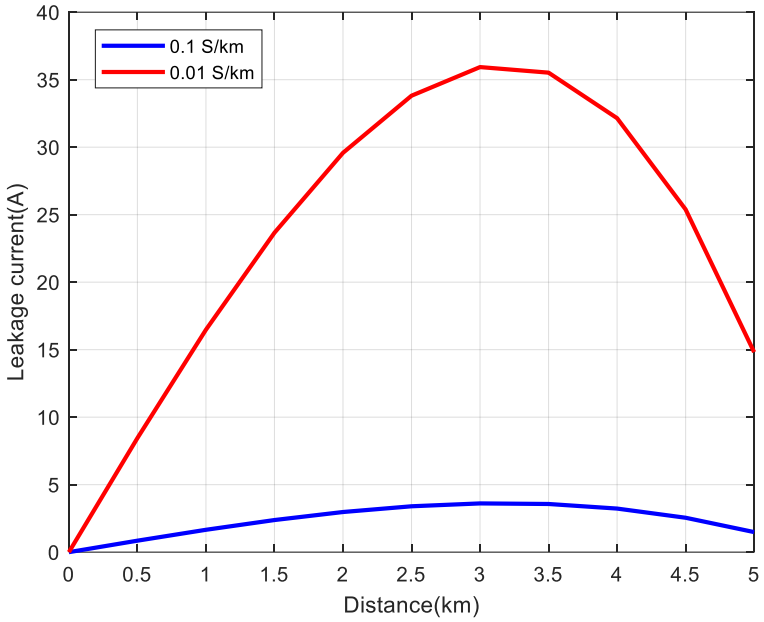

Figure 12. Results leakage current discrete model conductance between rail and earth 0.1 S/km and 0.01 S/km.

With the conductance between the rail and earth set at 0.01 S/km and 0.10 S/km using only the discrete model, the results of the analysis and comparison of leakage current simulations in (Table 3) and (Table 4) indicated that the leakage current dropped by an average of 89.96% and 89.95%, respectively. (Figure 12) shows the results of these findings.

3.2 Simulation SCCNS model

To simulate the SCCNS model, as shown in (Figure 5) and (Figure 6), matrix-based equations in equation (20) were used to examine the electric rail supply system's voltage and leakage current characteristics. The MATLAB/Simulink model creation tools are described in the appendix (Table 7), and the simulation parameters are listed in the appendix (Table 9). The appendix (Figure 20) illustrates how the SCCNS model was subsequently created for MATLAB/Simulink voltage and leakage current analysis. As shown in (Table 5), this system was simulated using MATLAB/Simulink to compare the outcomes with the discrete model. Furthermore, a comparison was made between the FNRCS model (cited in Topic 3.1) and the SCCNS model's simulation findings for rail voltage and leakage current. (Figure 13) shows the results of the simulation for rail voltage, and (Figure 14) shows the results for leakage current. As a result, comparing the simulations of the two models showed that the outcomes nearly matched and followed the same pattern.

Table 5. Results of the simulation for rail voltage and leakage current SCCNS model.

No.	Distance (km)	Rail voltage (V)		Leakage current (A) of Discrete model
		Discrete model	MATLAB/Simulink	
1	0	168.9875	168.9875	0.0000
2	0.50	160.5590	160.5590	8.4102
3	1.00	143.6984	143.6984	16.4016
4	1.50	118.3986	118.3986	23.5552
5	2.00	84.6490	84.6490	29.4512
6	2.50	42.4352	42.4352	33.6693
7	3.00	-8.2606	-8.2606	35.7877
8	3.50	-67.4599	-67.4599	35.3832
9	4.00	-135.1876	-135.1876	32.0309
10	4.50	-211.4725	-211.4725	25.3034
11	5.00	-296.3470	-296.3470	14.7708

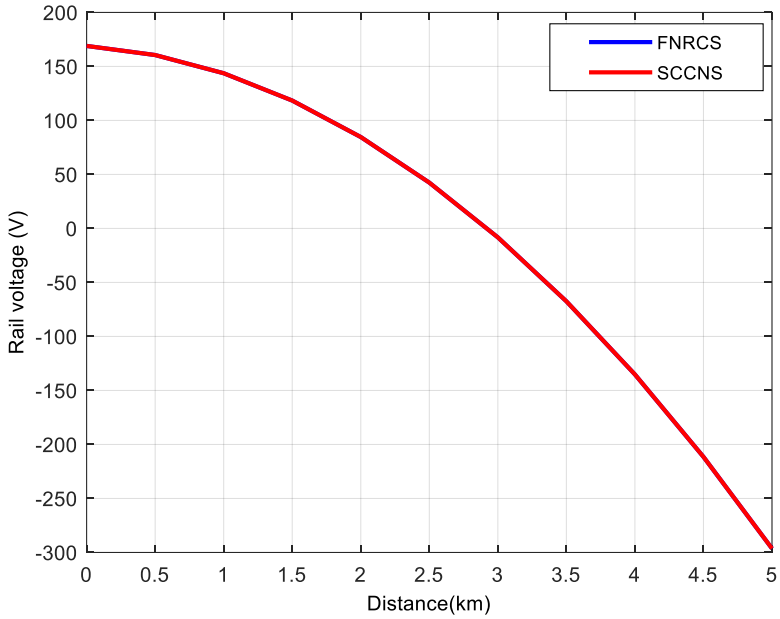

Figure 13. Results rail voltage between FNRCS and SCCNS model.

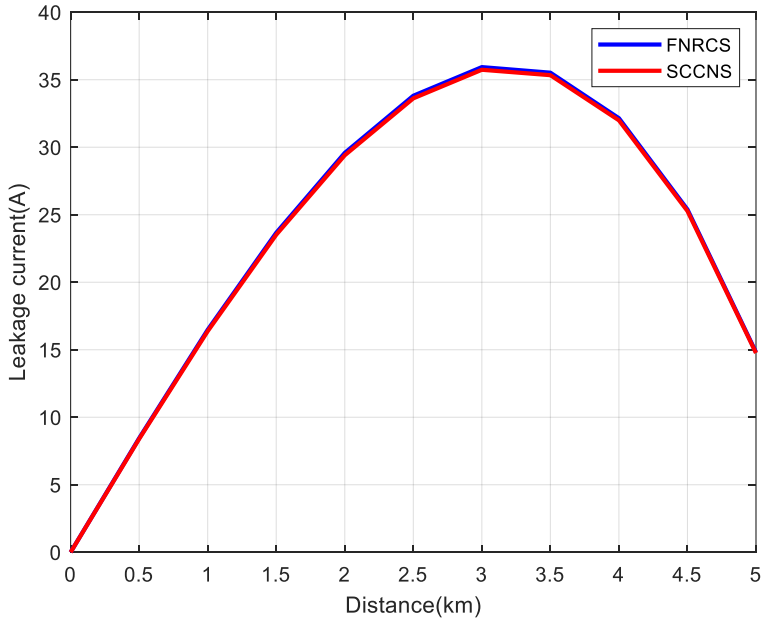

Figure 14. Results show the current leakage between the FNRCS and SCCNS models.

3.3 Simulation SCCNS with a drainage diode model

The voltage and leakage current characteristics in the electric rail supply system were analyzed using matrix-based calculations following equation (21) for the simulation of the SCCNS model with a drainage diode, as shown in (Figure 5) and (Figure 6). The appendix (Table 7) lists the MATLAB/Simulink tools used for model development, and the appendix (Table 10) provides specifics on the system parameters used for the simulation. As seen in the appendix (Figure 21), the SCCNS with a drainage diode model was then created to use MATLAB/Simulink to analyze rail voltage characteristics and leakage current characteristics. To compare the simulation results with the discrete model shown in (Table 6), this system was simulated using MATLAB/Simulink. Furthermore, the rail voltage and leakage current simulation results were compared

between the SCCNS with a drainage diode model and the FNRCS model, which was cited in (Topic 3.1). (Figure 15) and (Figure 16) show the results of the simulations for rail voltage and leakage current, respectively.

Table 6. Simulation results for rail voltage and leakage current SCCNS with a drainage diode model.

No.	Distance (km)	Rail voltage (V)		Leakage current (A) of Discrete model
		Discrete model	MATLAB/Simulink	
1	0	465.4235	465.3942	0.0000
2	0.50	456.9432	456.9140	2.3258
3	1.00	439.9824	439.9532	4.6093
4	1.50	414.5403	414.5110	6.8080
5	2.00	380.6157	380.5865	8.8798
6	2.50	338.2074	338.1782	10.7822
7	3.00	287.3134	287.2842	12.4729
8	3.50	227.9316	227.9024	13.9095
9	4.00	160.0596	160.0303	15.0496
10	4.50	83.6943	83.6650	15.8510
11	5.00	-1.1674	-1.1967	16.2712

A comparison between the FNRCS model and the SCCNS model with a drainage diode (Figure 15) revealed an average difference in the simulated rail voltage of 284.62 V. The voltage profile shows parallel lines with a downward slope. The FNRCS model exhibits a bell-shaped curve (Figure 16), showing the leakage current simulation results. On the other hand, the drainage diode model of the SCCNS shows a constant tendency to rise as the simulated distance grows. This shows an upward-sloping pattern in the leakage current in the SCCNS with a drainage diode model, increasing with the distance of the simulation from the substation starting point.

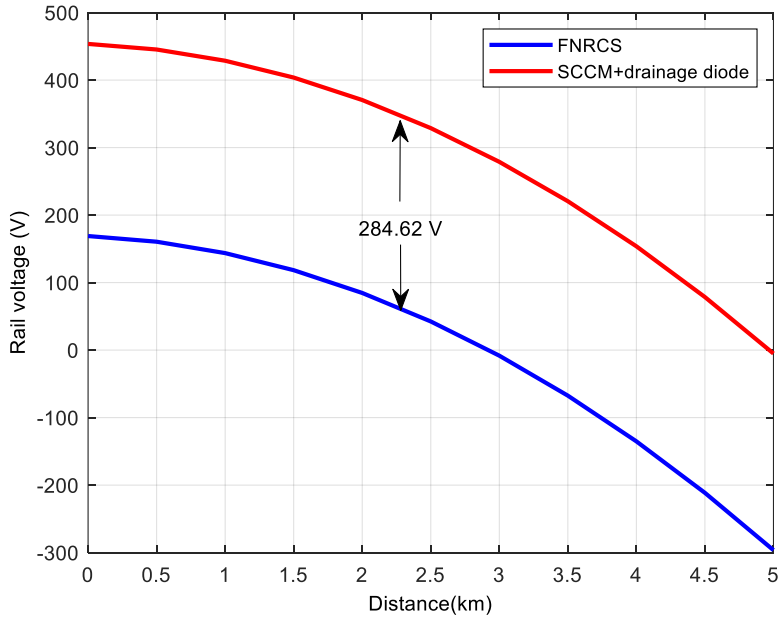

Figure 15. Results rail voltage between FNRCS and SCCNS with a drainage diode model.

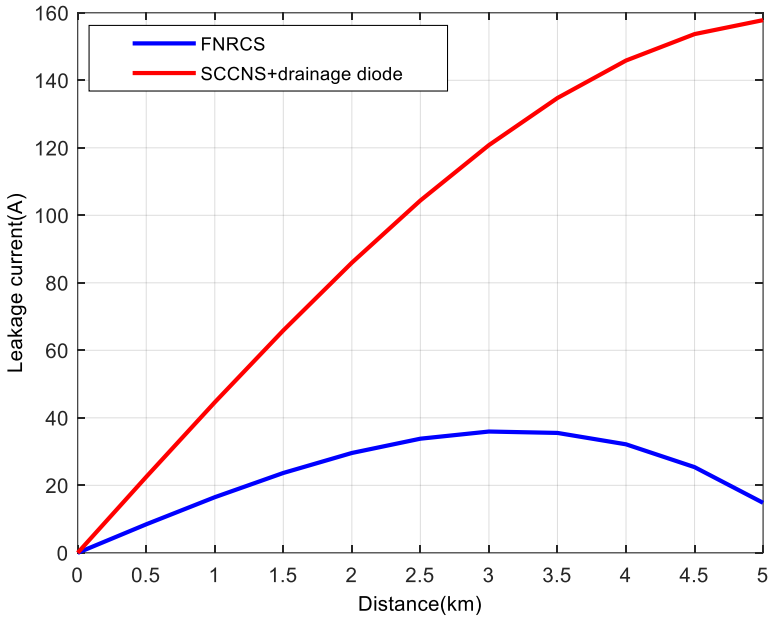

Figure 16. Results leakage current between FNRCS and SCCNS with a drainage diode model.

A comparison between the normal SCCNS model and the SCCNS with a drainage diode model was carried out to illustrate the variations in their simulation outcomes further. At a distance of 3.00 km, where the rail voltage is -0.25 V, it was discovered that the rail voltage profiles intersect. The rail voltage of the SCCNS with a drainage diode model is higher than that of the SCCNS model in the 0-3.00 km range. In contrast, (Figure 17) shows that the rail voltage of the SCCNS with a drainage diode model is lower than that of the SCCNS model in the 3.00–5.00 km range. The SCCNS model shows a bell-shaped curve for the leakage current simulation results (Figure 18). In contrast, the SCCNS with a drainage diode model shows a trend of continuous increase, which is comparable to the pattern seen in (Figure 16).

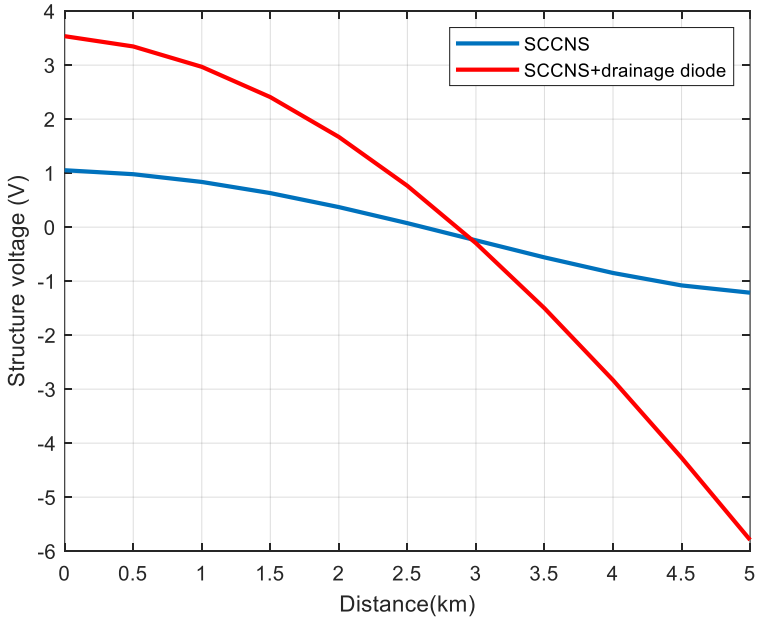

Figure 17. Results of the structure voltage between SCCNS and SCCNS with a drainage diode model.

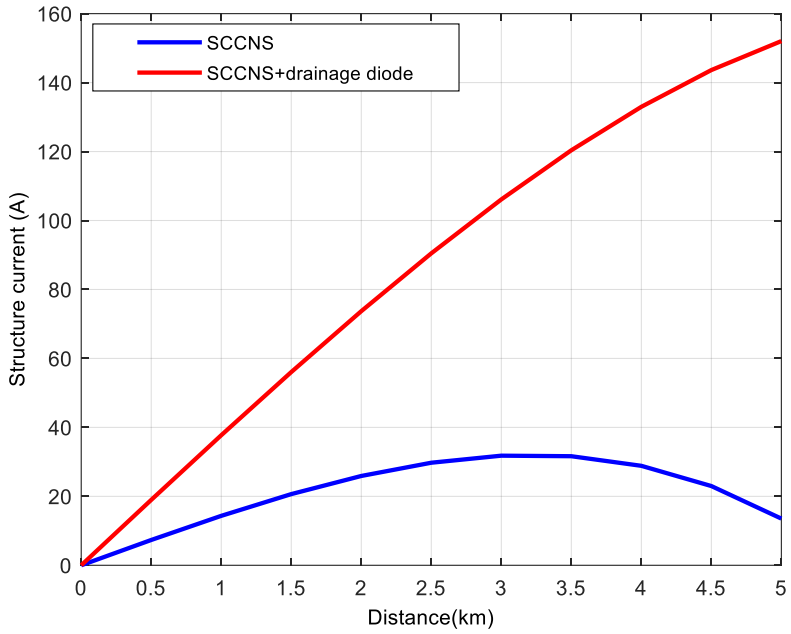

Figure 18. Results structure current between SCCNS and SCCNS with a drainage diode model.

3.4 Summary of simulation results

In this work, the railway power supply system's leakage current was analyzed utilizing simulations that handled huge and complicated parameters using MATLAB/Simulink. The simulation used three scenarios: the FNRCS model, the SCCNS model, and the SCCNS with a drainage diode model. The modeling, which took the shape of a single-line diagram and was created in MATLAB/Simulink for comprehensive simulation result analysis and verification, was based on the EN-50122-2 standard. Between the rail and the earth, conductance values of 0.01 S/km and 0.10 S/km were used to study the voltage and leakage current characteristics for the FNRCS model. The discrete model agreed with the MATLAB/Simulink simulation results. The average voltage deviation relative to the mathematical model was 8.47% for 0.10 S/km and 8.64% for 0.01 S/km. The simulation also revealed an average 40.07% increase in leakage current. Furthermore, an average of 89.96% and 89.95% were found in the leakage current when the conductance values of 0.01 S/km and 0.10 S/km were compared.

The voltage and leakage current characteristics of the SCCNS model were examined using matrix-based models. Regarding both voltage and leakage current behavior, the simulation results in MATLAB/Simulink closely matched the FNRCS model and agreed with the discrete model. The rail voltage for the SCCNS with a drainage diode model was 284.62 V on average, and the graph sloped downward like parallel lines. Three kilometers separated the voltage curves as compared to the SCCNS model. Compared to the SCCNS model, the rail voltage of the SCCNS with a drainage diode model was lower in the 3.00-5.00 km range and higher in the 0-3.00 km range. Furthermore, the bell-shaped curve seen in the SCCNS model contrasted the continuously growing trend of the leakage current in the SCCNS with a drainage diode model. It is clear from the simulation outcomes of the three scenarios that MATLAB/Simulink is a valuable tool for examining railway power supply systems. It offers precise simulation results and makes performance comparisons between various system models easy. The FNRCS, SCCNS, and SCCNS+Diode models are based on different simulation techniques that depend on their operational characteristics. FNRCS is ideal for mathematical modeling because of its continuous behavior. At the same time, SCCNS and SCCNS+Diode, which include switching elements and diodes, necessitate discrete modeling or the use of MATLAB/Simulink to represent their time-dependent behavior accurately. The highest flexibility is offered by MATLAB/Simulink, which supports both continuous and discrete systems, making it applicable to all types of networks with the correct simulation settings. The appendix (Table 11) presents the connection between each model and the simulation technique that corresponds to it.

4. Conclusions

The FNRCS model, the SCCNS model, and the SCCNS with a drainage diode model are the three models simulated in this work to analyze leakage current in the electric railway power supply system using MATLAB/Simulink. The models were created using the EN-50122-2 standard as a guide. According to the FNRCS model simulation results, the leakage current rose to 14.82 A while the rail voltage dropped from 169.90 V at the beginning to -297.38 V after 5 km. These findings, which had average variances of 8.47% for a conductance value of 0.10 S/km and 8.64% for 0.01 S/km, agreed with both the discrete and mathematical models. The average increase in leakage current over the mathematical model was 40.07%. The simulation results for leakage current and rail voltage for the SCCNS model closely matched those for the FNRCS model. The average rail voltage in the SCCNS with a drainage diode model was 284.62 V, indicating a steady declining trend; however, the leakage current dramatically increased with distance. The SCCNS with a drainage diode showed lower rail voltage in the 3.00-5.00 km range but greater rail voltage in the 0-3.00 km range than the SCCNS model. Overall, the simulation findings show that MATLAB/Simulink is a valuable tool for precisely evaluating and contrasting the performance of power supply systems for electric railways.

5. Acknowledgements

We thank Dr. Hidenori Shigeeda for his knowledge, support, and advice during this project. To ensure the practical completion of this study, Thaksin University, Phatthalung Campus, is also credited with providing the facilities required to perform the research utilizing MATLAB/Simulink software in the Faculty of Engineering.

Author Contributions: The simulation strategy and techniques were conceptualized and designed by T.C., S.K., and T.S. It was T.C. and S.K. who implemented the simulation, collected the data, analyzed the results, and came to a conclusion. The authors T.C., S.K., W.S., A.I., and T.S. contributed to the writing and the general content modification.

Funding: The National Research Council of Thailand (NRCT), Ministry of Higher Education, Science, Research, and Innovation, oversees the Researcher and Research for Industry Development Program (RRID), which provided funding for this study.

Conflicts of Interest: The authors of this study hereby state that they have no conflicts of interest.

References

[1] Bahra, K.S.; Catlow, R.B. Control of stray currents for DC traction systems. In International Conference on Electric Railways in a United Europe, Amsterdam, Netherlands, **1995**, pp. 136-142, https://doi.org/10.1049/cp:19950194.

[2] Siranec, M.; Regula, M.; Otcenasova, A.; Altus, J. Measurement and Analysis of Stray Currents. *In 20th International Scientific Conference on Electric Power Engineering (EPE), Kouty nad Desnou, Czech Republic*, **2019**, pp. 1-6, https://doi.org/10.1109/EPE.2019.8778072.

[3] Ogunsola, A.; Sandrolini, L.; Mariscotti, A. Evaluation of Stray Current From a DC-Electrified Railway With Integrated Electric–Electromechanical Modeling and Traffic Simulation. *IEEE Trans. Ind. Appl*. **2015**, 51, 5431-5441, https://doi.org/10.1109/TIA.2015.2429642.

[4] Niasati, M.; Gholami, A. Overview of stray current control in DC railway systems. In International Conference on Railway Engineering - Challenges for Railway Transportation in Information Age, Hong Kong, **2008**, pp. 1-6, https://doi.org/10.1049/ic:20080043.

[5] Petkova, P. Stray current control in DC railway systems. In 13th Electrical Engineering Faculty Conference (BulEF), Varna, Bulgaria, **2021**, pp. 1-3, https://doi.org/10.1109/BulEF53491.2021.9690814.

[6] Sutherland, P.E. Stray current analysis. *In IEEE IAS Electrical Safety Workshop, Toronto, ON, Canada*, **2011**, pp. 1-2, https://doi.org/10.1109/ESW.2011.6164732.

[7] Pham, K.D.; Thomas, R.S.; Stinger, W.E. Operational and safety considerations in designing a light rail DC traction electrification system. *In IEEE/ASME Joint Railroad Conference, Chicago, IL, USA*, **2003**, pp. 171-189, https://doi.org/10.1109/RRCON.2003.1204663.

[8] Petkova, P.; Boychev, B. Active stray current protection systems in DC railways. *In 13th Electrical Engineering Faculty Conference (BulEF), Varna, Bulgaria*, **2021**, pp. 1-3, https://doi.org/10.1109/BulEF53491.2021.9690843.
[9] Fotouhi, R.; Farshad, S. A new novel power electronic circuit to reduce stray current and rail potential in DC railway. *In 13th International Power Electronics and Motion Control Conference, Poznan, Poland*, **2008**, pp. 1575-1580, https://doi.org/10.1109/EPEPEMC.2008.4635491.
[10] Paul, D. DC Stray Current in Rail Transit Systems and Cathodic Protection [History]. *IEEE Ind. Appl. Mag*. **2016**, 22, 8-13, https://doi.org/10.1109/MIAS.2015.2481754.
[11] Tzeng, Y.-S.; Lee, C.-H. Analysis of Rail Potential and Stray Currents in a Direct-Current Transit System. *IEEE Trans. Power Deliv*. **2010**, 25, 1516-1525, https://doi.org/10.1109/TPWRD.2010.2040631.
[12] Hanrob, P.; Kulworawanichpong, T.; Ratniyomchai, T. Reducing Rail Potential and Stray Current with NEG-TPS in DC Electrified Railways. *In International Conference on Power, Energy and Innovations (ICPEI), Nakhon Ratchasima, Thailand*, **2021**, pp. 81-84, https://doi.org/10.1109/ICPEI52436.2021.9690665.
[13] Zaboli, A.; Vahidi, B. Stray Current and Rail Potential Control Strategies in Electric Railway Systems. In Transportation Electrification: Breakthroughs in Electrified Vehicles, Aircraft, Rolling Stock, and Watercraft, *IEEE*, **2023**, pp. 299-323, https://doi.org/10.1002/9781119812357.ch13.
[14] Hoger, M.; Regula, M.; Bracinik, P.; Otcenasova, A. Influence of high voltage power lines on the propagation of stray currents from DC traction. *In ELEKTRO, Krakow, Poland*, **2022**, pp. 1-5, https://doi.org/10.1109/ELEKTRO53996.2022.9803410.
[15] Liu, W.; Li, T.; Zheng, J.; Pan, W.; Yin, Y. Evaluation of the Effect of Stray Current Collection System in DC-Electrified Railway System. *IEEE Trans. Veh. Technol*. **2021**, *70*, 6542-6553, https://doi.org/10.1109/TVT.2021.3084340.
[16] Mariscotti, A. Stray Current Protection and Monitoring Systems: Characteristic Quantities, Assessment of Performance and Verification. *Sensors* **2020**, *20*, 6610. https://doi.org/10.3390/s20226610.
[17] Liang, H.; Wu, Y.; Han, B.; Lin, N.; Wang, J.; Zhang, Z.; Guo, Y. Corrosion of Buried Pipelines by Stray Current in Electrified Railways: Mechanism, Influencing Factors, and Protection. *Appl. Sci*. **2025**, *15*, 264. https://doi.org/10.3390/app15010264.
[18] Georgiev, V.; Petkova, P. Modeling of the influence of different parameters of the power supply system on the magnitude of the stray currents in DC electrified transport. *In 13th Electrical Engineering Faculty Conference (BulEF), Varna, Bulgaria*, **2021**, pp. 1-6, https://doi.org/10.1109/BulEF53491.2021.9690818.
[19] Yu, J.G.; Goodman, C.J. Modelling of rail potential rise and leakage current in DC rail transit systems. *In IEE Colloquium on Stray Current Effects of DC Railways and Tramways, London, UK*, **1990**, pp. 2/2/1-2/2/6.
[20] Lin, S.; Tang, Z.; Chen, X.; Liu, X.; Liu, Y. Analysis of Stray Current Leakage in Subway Traction Power Supply System Based on Field-Circuit Coupling. *Energies* **2024**, *17*, 3121. https://doi.org/10.3390/en17133121.
[21] Lee, C.-H.; Lu, C.-J. Assessment of grounding schemes on rail potential and stray currents in a DC transit system. *IEEE Trans. Power Deliv*. **2006**, 21, 1941-1947, https://doi.org/10.1109/TPWRD.2006.874561.
[22] Tang, Z.; et al. The Influence of Urban Rail Transit's Stray Current on Power Grid and Its Synchronous Monitoring. *In IEEE 4th Conference on Energy Internet and Energy System Integration (EI2), Wuhan, China*, **2020**, pp. 308-312, https://doi.org/10.1109/EI250167.2020.9346946.
[23] Sopharak, A.; Ratniyomchai, T.; Kulworawanichpong, T. Energy Saving Study of Mass Rapid Transit by Optimal Train Coasting Operation. *In International Conference on Power, Energy and Innovations (ICPEI), Chiangmai, Thailand*, **2020**, pp. 25-28, https://doi.org/10.1109/ICPEI49860.2020.9431507.
[24] Ratniyomchai, T.; Hillmansen, S.; Tricoli, P. Optimal capacity and positioning of stationary supercapacitors for light rail vehicle systems. *In International Symposium on Power Electronics, Electrical Drives, Automation and Motion, Ischia, Italy*, **2014**, pp. 807-812, https://doi.org/10.1109/SPEEDAM.2014.6872019.
[25] Zhao, Y.; Xu, J.; Yin, J. Urban rail transit line and station planning optimization based on GIS: Take Haikou city as an example. *In International Conference on Information Control, Electrical Engineering and Rail Transit (ICEERT), Lanzhou, China*, **2021**, pp. 240-247, https://doi.org/10.1109/ICEERT53919.2021.00053.
[26] Radu, P.V.; Lewandowski, M.; Szelag, A.; Steczek, M. Short-Circuit Fault Current Modeling of a DC Light Rail System with a Wayside Energy Storage Device. *Energies* **2022**, 15, 3527. https://doi.org/10.3390/en15103527.
[27] Colella, P.; Pons, E.; Tortora, A. Rail Potential Calculation: Impact of the Chosen Model on the Safety Analysis. *In AEIT International Annual Conference, Bari, Italy*, **2018**, pp. 1-6, https://doi.org/10.23919/AEIT.2018.8577295.

[28] Kirawanich, P.; Dey, P.; Sumpavakup, C. System-Level Magnetic Interference Modeling in Electrified Monorail System for Track-Side Safety Design. *IEEE Trans. Transp. Electrif.* **2024**, *10*, 4571-4582, https://doi.org/10.1109/TTE.2023.3306999.

[29] Yuan, P.; Mao, W.; Ye, H.; Liu, Y. Model Construction and Analysis of Transformer DC Magnetic Bias Induced by Rail Transit Stray Current. *In IEEE 3rd Conference on Energy Internet and Energy System Integration (EI2), Changsha, China*, **2019**, pp. 1710-1713, https://doi.org/10.1109/EI247390.2019.9061729.

[30] Shao, H.; Yang, X.; He, Y.; Zheng, T.Q. Stray Current and Rail Potential Dynamic Emulator for Urban Rail Transit System. *In IEEE Transportation Electrification Conference & Expo (ITEC), Detroit, MI, USA*, **2023**, pp. 1-6, https://doi.org/10.1109/ITEC55900.2023.10186932.

[31] Kangguan, K.; Hong, S.; Xinde, Z.; Xing, W.; Fan, Z.; Zhuohong, P. Development of a Stray Current Testing Device Based on Harmonic Current Source Technology. *In IEEE International Conference on High Voltage Engineering and Applications (ICHVE), Chongqing, China*, **2022**, pp. 1-4, https://doi.org/10.1109/ICHVE53725.2022.9961760.

[32] Gu, J.; Yang, X.; Zheng, T.Q.; Xia, X.; Zhao, Z.; Chen, M. Rail Potential and Stray Current Mitigation for Urban Rail Transit With Multiple Trains Under Multiple Conditions. *IEEE Trans. Transp. Electrif.* **2022**, *8*, 1684-1694, https://doi.org/10.1109/TTE.2021.3114412.

[33] White, R.D. AC/DC railway electrification and protection. *In IEE ETS Supply AC & DC* 2006, pp. 281-322, https://doi.org/10.1109/ICHVE53725.2022.9961760.

[34] Kiessling, F.; Puschman, R.; Schmieder, A.; Schneider, E. Contact lines for electric railways, SEIMENS, Publicis Publishing, 2nd edition, **2009**.

[35] Lu, S. Optimising power management strategies for railway traction. PhD Thesis, University of Birmingham, **2011**.

[36] Kaewpoung, S.; Sumpavakup, C.; Kulworawanichpong, T. Autotransformer-fed railway power supply model using. *In Advances in Future Manufacturing Engineering: Proceedings of the 2014 International Conference on Future Manufacturing Engineering (ICFME 2014), Hong Kong, December 10-11*, **2014**, *2*, https://doi.org/10.1201/b18474-4.

Supplement Materials

Detailed information regarding the several toolboxes utilized for MATLAB/Simulink model development may be found in the research's supplemental appendix. The parameter settings utilized to simulate the analysis results of the FNRCS, SCCNS, and SCCNS with drainage diode models are also included; these are shown in the following tables and figures.

Table 7. Components of a simulation in the MATLAB/Simulink program.

Toolbox	Details	Simulink Library Browser
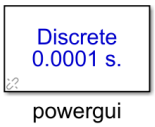	powergui	Simscape->Power Systems->Spacialized Technology ->Fundametal Blocks
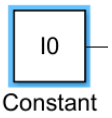	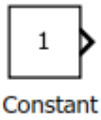	Simulink->Sources
	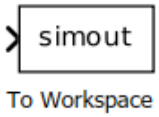	Simulink->Sinks
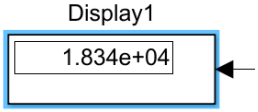	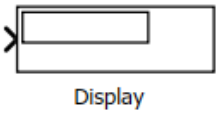	Simulink->Sinks
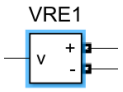		Simscape->Power Systems->Spacialized Technology -> Fundametal Blocks->Measurements
	Ground	Simscape->Power Systems->Spacialized Technology-> Fundametal Blocks->Elements
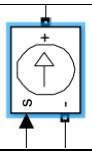	Controlled Current Source	Simscape->Power Systems->Spacialized Technology->Fundametal Blocks->Electrical Sources
	Series RLC Load	Simscape->Power Systems->Spacialized Technology->Fundametal Blocks->Power Electronics
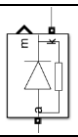	Didoe	Simscape->Power System->Spacialized Technology->Fundametal Blocks->Element

Table 8. Parameter for simulation of FNRCS model.

Parameter	Value
Current at Substation (I_0)	10.00 kA
Distance (L)	5.00 km
Sampling (dx)	0.50 km
Rail resistance (R'_R)	0.017 Ω/km
Conductance between rail and earth (G'_{RE})	0.10 S/km, 0.01 S/km

Table 9. Parameter for simulation of SCCNS model.

Parameter	Value
Current at Substation (I_0)	10.00 kA
Distance (L)	5.00 km
Sampling (dx)	0.50 km
Rail resistance (R'_R)	0.017 Ω/km
Conductance between rail and earth (G'_{RE})	0.10 S/km, 0.01 S/km
R'_{SCCNS}	0.02 Ω/km
R_E or G'_E	0.50 Ω/km or 2.00 S/km

Table 10. Parameter for simulation of SCCNS with drainage diode model.

Parameter	Value
Current at Substation (I_0)	10.00 kA
Distance (L)	5.00 km
Sampling (dx)	0.50 km
Rail resistance (R'_R)	0.017 Ω/km
Conductance between rail and earth (G'_{RE})	0.10 S/km, 0.01 S/km
R'_{SCCNS}	0.02 Ω/km
R_E or G'_E	0.50 Ω/km or 2.00 S/km
V_{diode}	0.70 V

Table 11. Model usage for FNRCS/SCCNS/SCCNS+diode systems.

Model	FNRCS	SCCNS	SCCNS+diode
Mathematical	Yes	No	No
Discrete models	Yes	Yes	Yes
MATLAB/Simulink	Yes	Yes	Yes

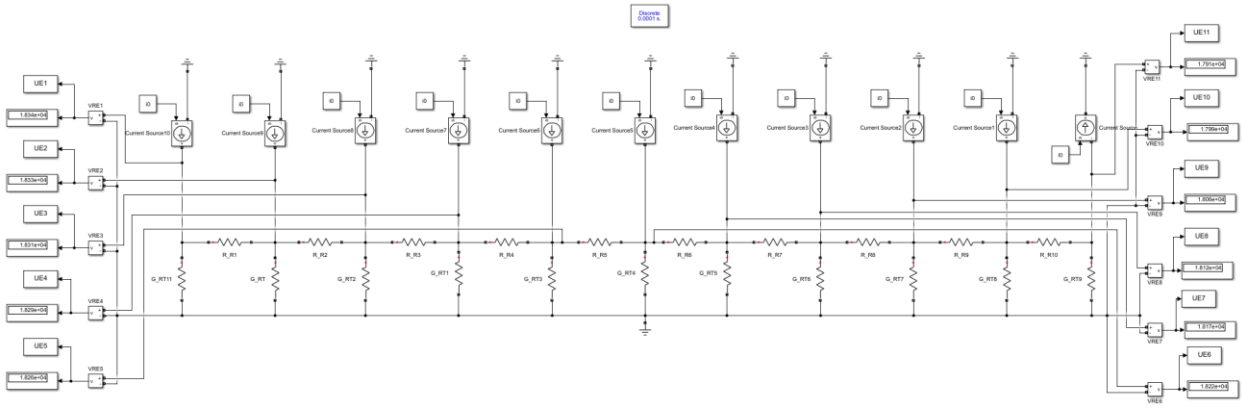

Figure 19. Development FNRCS model in the MATLAB/Simulink program.

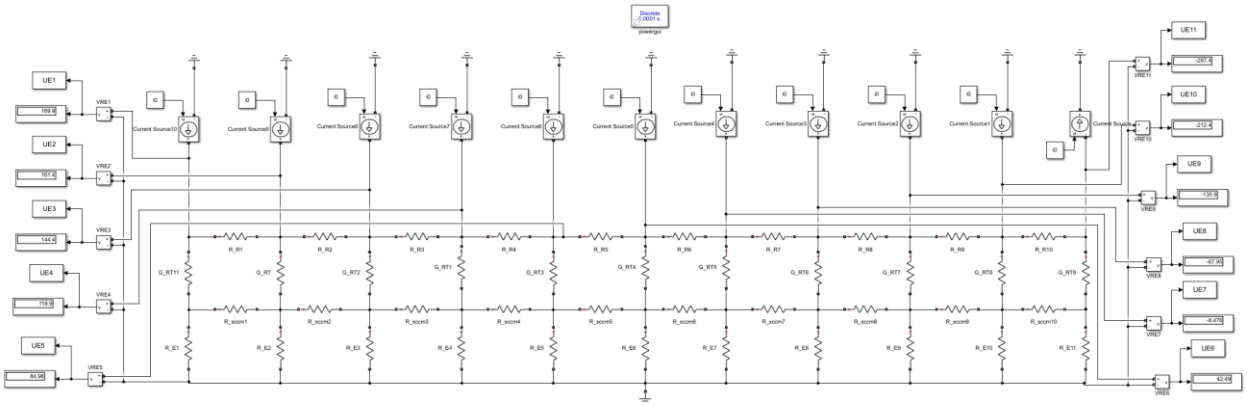

Figure 20. Development SCCNS model in the MATLAB/Simulink program.

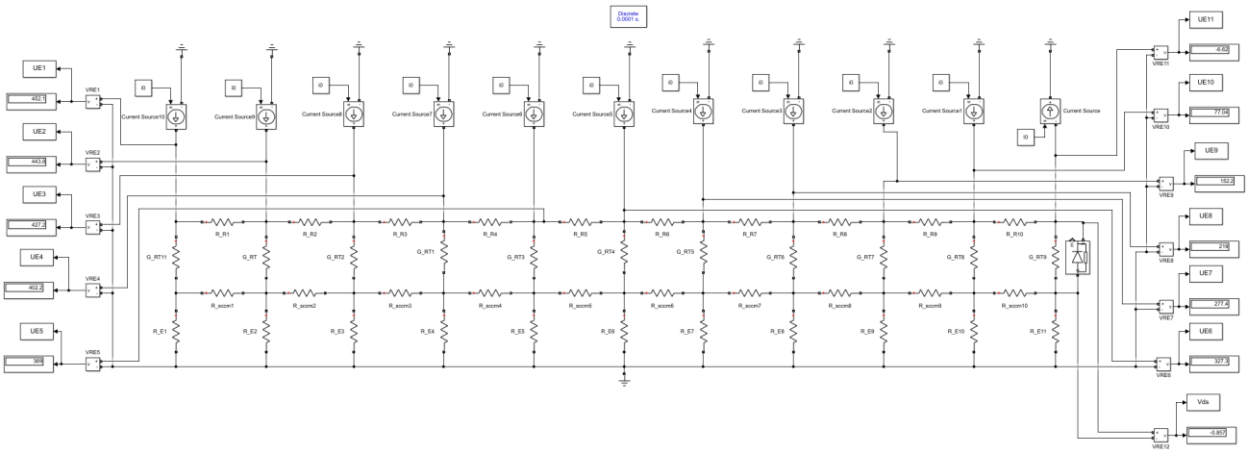

Figure 21. Development of SCCNS with drainage diode model in the MATLAB/Simulink program.